ChemMedChem

Research Article
doi.org/10.1002/cmdc.202300662

Chemistry Europe
European Chemical Societies Publishing

www.chemmedchem.org

Iodinated 4,4′-Bipyridines with Antiproliferative Activity Against Melanoma Cell Lines

Paola Peluso,*[a] Victor Mamane,*[b] Ylenia Spissu,[c] Giuseppina Casu,[d] Alessandro Dessì,[a] Roberto Dallocchio,[a] Barbara Sechi,[a] Giuseppe Palmieri,[d] and Carla Rozzo*[d]

In the last decade, biological processes involving halogen bond (HaB) as a leading interaction attracted great interest. However, although bound iodine atoms are considered powerful HaB donors, few iodinated new drugs were reported so far. Recently, iodinated 4,4′-bipyridines showed interesting properties as HaB donors in solution and in the solid state. In this paper, a study on the inhibition activity of seven halogenated 4,4′-bipyridines against malignant melanoma (MM) cell proliferation is described. Explorative dose/response proliferation assays were first performed with three 4,4′-bipyridines by using four MM cell lines and the normal BJ fibroblast cell line as control. Among them, the A375 MM cell line was the most sensitive, as determined by MTT assays, which was selected to evaluate the antiproliferative activity of all 4,4′-bipyridines. Significantly, the presence of an electrophilic iodine impacted the biological activity of the corresponding compounds. The 3,3′,5,5′-tetrachloro-2-iodo-4,4′-bipyridine showed significant antiproliferation activity against the A375 cell line, and lower toxicity on BJ fibroblasts. Through *in silico* studies, the stereoelectronic features of possible sites determining the bioactivity were explored. These results pave the way for the utilization of iodinated 4,4′-bipyridines as templates to design new promising HaB-enabled inhibitors of MM cell proliferation.

Introduction

The incidence of cutaneous malignant melanoma (CMM) is steadily increasing in the population from Western countries, though it is fortunately diagnosed at an early stage of disease – defined as having a low tumor thickness – in most cases and, thus, being effectively treated by surgical excision.[1] The malignant proliferation of melanocytes, which are the cells responsible for melanin production, underlies onset and development of this disease. Despite the impressive advancements into the treatment of the disease during the last decade, with integration of the different therapeutic approaches available (surgery, radiotherapy, immunotherapy, target therapy, and chemotherapy), a large fraction of advanced stages remains refractory to systemic therapies.[2] Moreover, clinical outcome is difficult to predict in melanoma patients due to the marked heterogeneity of the disease from the biological and molecular point of view.[3] Overall, given that long-term survival is achieved in only about 50% of patients with metastatic melanoma, development of new effective pharmacological therapies remains of great interest in the field of cancer research.[4,5]

The main approaches for research and discovery of new drugs against melanoma are based on *in silico*, 2D and 3D *in vitro*, and *in vivo* models.[6] Among them, structure- and ligand-based drug design exploit *in silico* approaches focusing on noncovalent interactions to identify and optimize potential drugs and their interactions with biomacromolecular hosts.[7]

In biological systems, hydrogen bonds (HBs), dipole-dipole and π-π interactions, and coulombic forces[8–10] are considered the most frequent intermolecular noncovalent interactions acting to promote and regulate drug action at different levels including absorption, transport, and distribution in the living body, metabolism, pharmacokinetics, pharmacodynamics, and excretion.[8a] More recently, halogen (HaB),[11] chalcogen,[12] spodium[13] and π-hole[14] bonds were also identified as interactions underlying ligand-protein binding, recognition, and function. These achievements have paved the way for new horizons in drug design and discovery.[8a,15,16] On the other hand, over the past decades drug discovery research deviated away from natural products,[17] and new forms of noncovalent interactivity may orientate drug design towards unexplored regions of the chemical space. This remains an urgent issue given that, although the theoretically existing chemical space is extremely vast, the chemical space that is effectively explored in drug discovery is limited.

[a] Dr. P. Peluso, A. Dessì, R. Dallocchio, B. Sechi
Istituto di Chimica Biomolecolare ICB-CNR
Consiglio Nazionale delle Ricerche (CNR)
Traversa La Crucca, 3, Li Punti, 07100 Sassari, Italy
E-mail: paola.peluso@cnr.it

[b] Dr. V. Mamane
Institut de Chimie de Strasbourg, UMR CNRS 7177
Centre National de la Recherche Scientifique (CNRS)
1 Rue Blaise Pascal, 67008 Strasbourg, France
E-mail: vmamane@unistra.fr

[c] Dr. Y. Spissu
Istituto di Scienze delle Produzioni Alimentari ISPA-CNR
Consiglio Nazionale delle Ricerche (CNR)
Traversa La Crucca, 3, Li Punti, 07100 Sassari, Italy

[d] G. Casu, Prof. G. Palmieri, Dr. C. Rozzo
Istituto di Ricerca Genetica e Biomedica IRGB-CNR
Consiglio Nazionale delle Ricerche (CNR)
Traversa La Crucca, 3, Li Punti, 07100 Sassari, Italy
E-mail: carlamaria.rozzo@cnr.it

Supporting information for this article is available on the WWW under https://doi.org/10.1002/cmdc.202300662

In the last few years, HaB has especially attracted great interest in drug discovery.[11,18] In Figure 1, the concept of HaB is described considering a possible HaB between fluoroiodine and acetone, as representative example, and the electrostatic potential isosurfaces (V_S) of the interacting species to highlight the electronic bases of the interaction (color legend: blue, electrophilic region featuring low electron charge density; red, nucleophilic region featuring high electron charge density). The HaB originates from the anisotropic charge distribution which features bound halogens.[19] This electron anisotropy determines the amphoteric behavior of bound halogens given that an area of lower electron charge density (δ^+), the σ-hole, located on the elongation of the covalent bond, coexists with an area of higher electron charge density (δ^-), which forms a belt orthogonal to the covalent bond. Thus, halogen atoms behave either as Lewis bases through their negative belt, or as Lewis acids through their σ-hole. The electrophilic properties of these HaB donors allow them to interact with a nucleophile acceptor. The most important features of the HaB are directionality and tunability. Given that the strength of a HaB increases as the polarizability and the electronegativity of the halogen increases and decreases, respectively, iodine is considered a powerful HaB donor, particularly when it is bound to electron-withdrawing groups or atoms, like the fluorine atom. In this case, the electron charge density is polarized toward the electron-withdrawing atom, increasing the depletion of electron charge density on the bound halogen (iodine).

Most evidence about HaBs involving iodine atoms in biological contexts has been derived from the crystallographic structures of ligand-protein complexes reported in the Protein Data Bank (PDB) and confirmed by computational analysis.[20,21] In these complexes, oxygen atoms belonging to protein backbone and sidechains are the most frequent sites profiled as HaB acceptors. On this basis, recent studies have shown that fragments containing halogen atoms, potentially able to exert HaB,[11b] bind more often to proteins than non-halogenated fragments,[22] and halogenated libraries provided interesting hits for lead generation.[23] Bound iodine atoms present remarkable properties as HaB donors; thus, their presence in halogenated fragments is very important. Despite that, this heavy halogen remains underrepresented in drug discovery,[18d] and design, synthesis and application of new iodinated compounds was reported in less degree so far. In fact, only 1.4% of the halogenated drugs available in the market are iodinated compounds.[20]

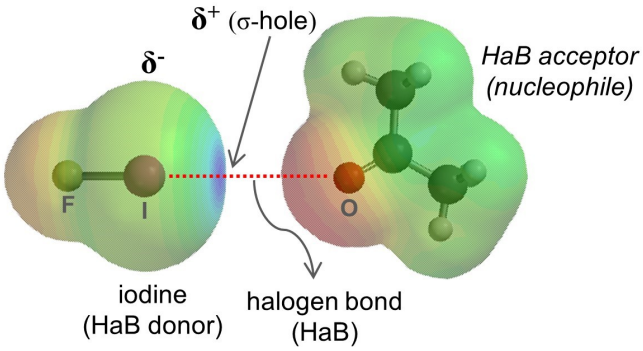

Figure 1. Description of HaB by considering a possible I···O interaction between fluoroiodine and acetone. V_S representations on electron density isosurfaces (0.002 au), graphically generated by using Spartan' 10 (DFT/B3LYP/6-31G*) (color legend for V_S isosurfaces: blue, electrophilic region featuring low electron charge density; red, nucleophilic region featuring high electron charge density; other colors, regions with intermediate values of *V*) (color legend for ball and stick structures: grey, C; yellow, F; pale grey, H; magenta, I; red, O).

The interest toward iodinated compounds is not unusual in melanoma research. Halogenated drugs were shown to be potent inhibitors of mutated BRAF.[24] Single point mutagenesis experiments and computational analysis indicated that HaB may play a role in determining the inhibition activity. Recently, Kozyra et al. studied a series of thiosemicarbazide derivatives, showing that the activity of the derivatives against melanoma cell line G-361 increased in the given series of substituents following the order 2-bromophenyl < naphth-1-yl < 2-iodophenyl < 4-methylthiophenyl < 4-iodophenyl.[25] Furthermore, iodinated compounds such as iodothiouracils, iodoquinolines, and iodobenzamides have been used as imaging and radiotherapeutic agents for malignant melanoma. In this regard, the biodistribution and pharmacokinetic profile of [^{123}I]iodobenzamides were found greatly influenced by the substituents on the benzene ring, while the uptake values in the tumor correlated with molecule's lipophilicity.[26,27]

Given this context, the study described herein represents a proof-of-principle exploration aiming to investigate the effectiveness of new iodinated compounds against melanoma cell lines. For this purpose, we explored the antiproliferative activity of the iodinated 3,3′,5,5′-tetrachloro-4,4′-bipyridines **1**–**5** (Table 1) against melanoma cells in terms of dose and time dependence, and the capability of inducing apoptosis was considered. The antiproliferative activity of 3,3′,5,5′-tetrachloro-4,4′-bipyridines **6** and **7**, as non-iodinated references for comparison, was also explored. Compounds **1**–**7** were considered as test probes inside the cells to explore the effect of specific functional groups on the antiproliferative activity against melanoma cells, and on the cytotoxicity toward fibroblasts. For this purpose, the substitution pattern of the series could be correlated by means of the subtle addition, deletion, or modification of distinctive functional groups, as shown in Table 1.

By using electrostatic potential (*V*) analysis, a second aim of the study was to demonstrate that the antiproliferative activity, at molecular level, may be correlated with the electrophilic properties of iodine.

We hypothesized that the formation of HaBs involving the iodine atoms of the 4,4′-bipyridines and carbonyl oxygens of protein backbone could underlie the antiproliferative activity of the heterocyclic derivatives against melanoma cell lines (Figure 2).

Table 1. Structures of compounds **1**–**7** highlighting the distinctive functional groups, and list of subtle addition, deletion, or modification of distinctive functional groups summarizing the structural relationships within the series.

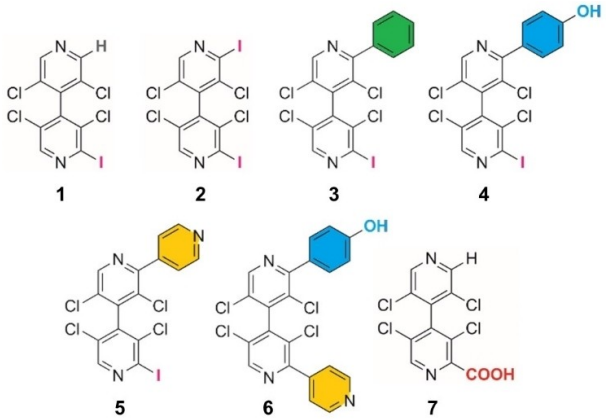

Compound	Functional group modification
1↔**2**	H↔I
1↔**7**	I↔COOH
1↔**3**	H↔Phenyl
1↔**4**	H↔C_6H_4OH
1↔**5**	H↔C_5H_4N
2↔**3**	I↔Phenyl
2↔**4**	I↔C_6H_4OH
2↔**5**	I↔C_5H_4N
2↔**6**	I↔C_6H_4OH; I↔C_5H_4N
3↔**4**	Phenyl↔C_6H_4OH
3↔**5**	Phenyl↔C_5H_4N
4↔**6**	I↔C_5H_4N
5↔**6**	I↔C_6H_4OH

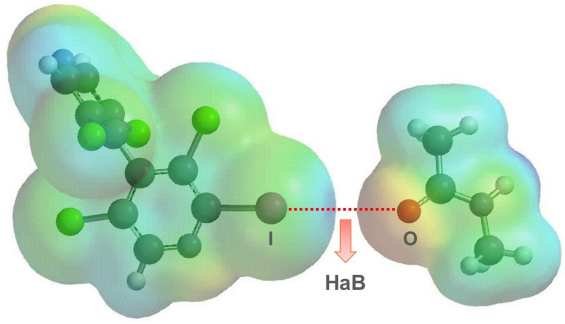

Figure 2. Possible HaB between the iodine atom of compound **1** and the *N*-methyl acetamide, as a simplified model of the protein carbonyl oxygen. V_S representations on electron density isosurfaces (0.002 au), graphically generated by using Spartan' 10 (DFT/B3LYP/6-31G*) (color legend for V_S isosurfaces: blue, electrophilic region featuring low electron charge density; red, nucleophilic region featuring high electron charge density; other colors, regions with intermediate values of *V*) (color legend for ball and stick structures: grey, C; green, Cl; pale grey, H; magenta, I; violet, N; red, O).

Results and Discussion

Iodinated 4,4′-Bipyridines as Potential Anticancer Agents

The 4,4′-bipyridine core is a powerful electron-withdrawing group, which is able to enhance the electrophilic properties of bound halogens, thus increasing their ability as HaB donors.[28] On this basis, iodinated 4,4′-bipyridines were designed by Peluso and Mamane groups as test probes with HaB-enabled functions which were confirmed in both chemical and biochemical environment.[28] Indeed, the 4,4′-bipyridyl unit exerts an electron-withdrawing effect on the bound iodine atom, increasing its electrophilic properties and ability as HaB donor.[28] As a result, this family of compounds proved to be efficient HaB donors at the solid state by X-ray diffraction analysis,[28a] in separation science,[29] and as inhibitors of transthyretin (TTR) fibrillogenesis *in vitro*.[28b] In this latter case, TTR was used as benchmark protein with well-known ability to bind iodinated ligands, like thyroxine, by HaB.[30]

Using nitrogen heterocycles presented additional advantages. Indeed, nitrogen is known to be a high-impact design element in drug design because substitution of a CH group with a N atom, in aromatic and heteroaromatic ring frameworks, often improves the pharmacological profile of a molecular structure at different levels.[31] Furthermore, the two pyridyl nitrogen atoms could work as HB acceptors. In terms of pharmacological properties, the 4,4′-bipyridyl system was used to prepare the supramolecular dimetallic *trans*-(Pt-(II)(salicylaldimine))$_2$(4,4′-bipyridine) $2BF_4$ complex which showed *in vitro* anticancer effect comparable to cisplatin in breast (MCF-7) and liver (HepG2) cancer cells.[32] Moreover, anticancer activity was reported for a series of 4,4′-bipyridinium amphiphiles that, *in vitro*, showed IC_{50} values in the low-micromolar range against human cancer cells and the cisplatin resistant A549 cancer cells.[33]

Another interesting feature of substituted 4,4′-bipyridines is the possibility to introduce chirality in their structure. In this regard, compounds **2**–**6** are chiral for atropisomerism, namely for restricted rotation around the 4,4′-bond (chiral axis), whereas compounds **1** and **7** feature C_2 symmetry and are not chiral. Although enantioselective bioactivity was not considered in the study described herein, axial chirality can be used as a tool for finely tuning the antiproliferative activity of these compounds. Indeed, several studies demonstrated that in many cases control of atropisomeric conformation may be used as a general strategy to improve the selectivity profile of potential drugs.[34] Furthermore, several atropisomeric structures, in both racemic and enantiopure forms, attracted interest in anticancer research. For instance, the natural product Gossypol and its derivatives were studied as Bcl-2 inhibitors, this system showing marked enantioselective anticancer effects.[35] The atropisomeric forms of Dabrafenib interact enantioselectively with its primary target BRAF.[36] In the last few years, Palmieri and Rozzo group studied the antiproliferative activity of a large series of functionalized curcumin-like 1,1′-biphenyls, showing that hydroxylated biphenyl derivatives bearing an α,β-unsaturated ketone are

excellent "lead compounds" for the potential development of drugs that may be useful for treating malignant melanoma.[37]

Synthesis of 4,4′-Bipyridines 1–7

Molecular structures identified for *de novo* development of new drugs must be synthetically accessible, easy to be functionalized, and with high interactive potentialities.[38] Thus, to explore new regions of the chemical space in drug discovery, the availability of versatile synthetic strategies to access series of structural analogues by subtle modifications of a lead scaffold is essential. Indeed, different biological responses could be associated with subtle stereoelectronic differences as a functional group changed.

Compounds **1**–**7** bearing different substituents at the 2,2′-positions were prepared in few steps from 3,5-dichloropyridine (**8a**) and 2-bromo-3,5-dichloropyridine (**8b**) as starting materials (Scheme 1). First, the base-induced dimerization of pyridines **8a**,**b** furnished the corresponding polyhalogenated 4,4′-bipyridines **9a**,**b** (reaction conditions a).[28a] Bipyridine **9b** was then used for the preparation of compound **2** through a diamino-copper-catalyzed aromatic Finkelstein reaction (conditions b).[28a] During this reaction, compound **1** could be also isolated as a minor product.[28b] The latter could be selectively prepared from bipyridine **9a**. After mono-*N*-oxydation (conditions c), the obtained bipyridine oxide **10** was transformed to bipyridine **11** (conditions d)[28c] which was submitted to a final Finkelstein reaction to afford compound **1** (condition b). For compounds **3**–**6**, the previously reported methodology for their synthesis was improved. Indeed, their preparation was based on non-selective palladium-catalyzed Suzuki reactions involving compound **2**, generating low yields with tedious chromatographic separations.[28b] Herein, we used the key intermediate **12** bearing non-equivalent halogens in 2- and 2′-positions to provide more selective cross-coupling reactions. The unsymmetrical bipyridine **12** was prepared from bipyridine **11** through a sequence comprising selective oxidation of the less hindered

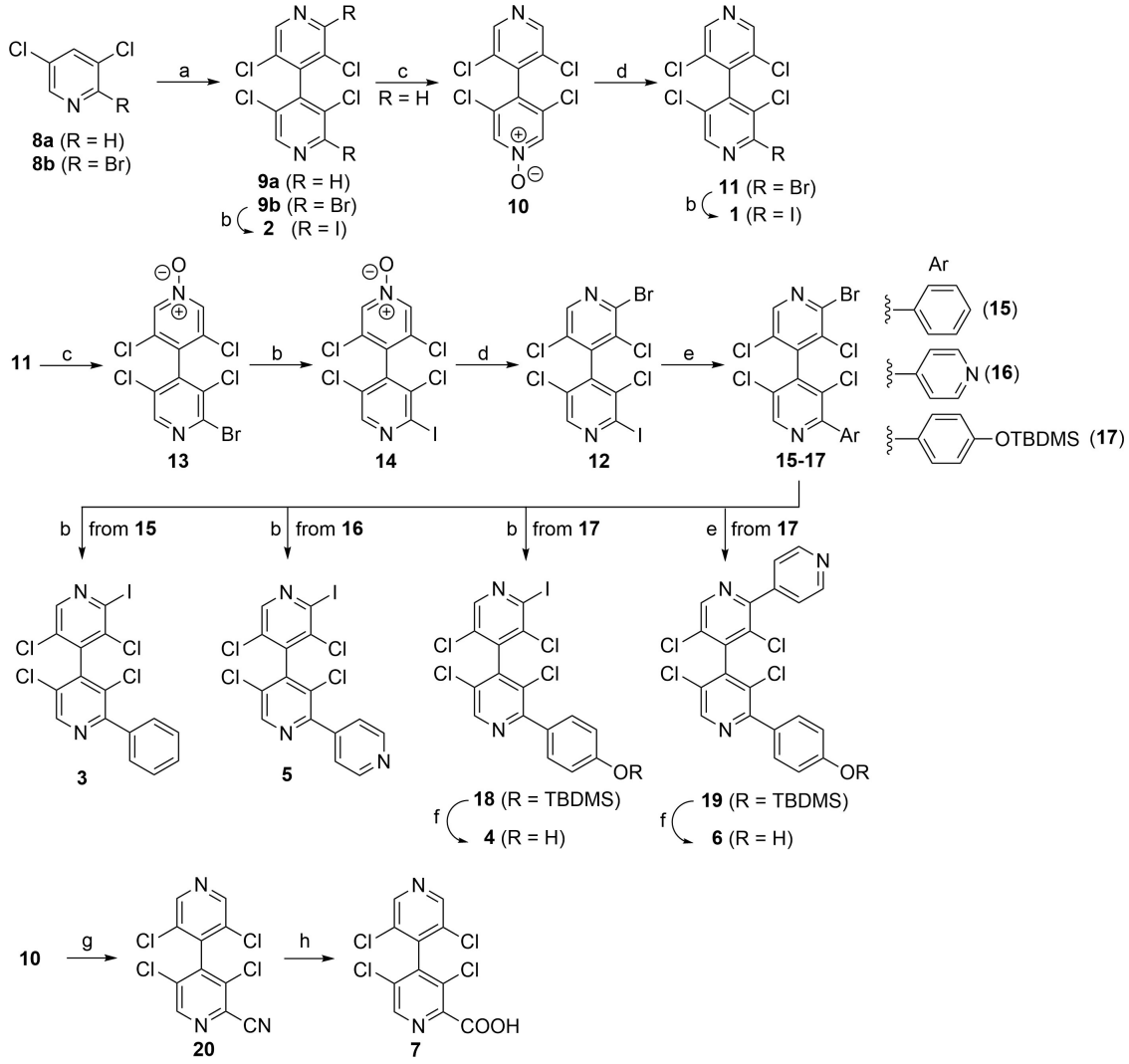

Scheme 1. Preparation of compounds **1**–**7**. (a) LDA, THF, −45 to −10 °C then I_2. (b) NaI, CuI, *trans*-*N*,*N*′-dimethylcyclohexane-1,2-diamine, dioxane, 120 °C. (c) *m*-CPBA, CH_2Cl_2, rt. (d) $(COBr)_2$, CH_2Br_2, Et_3N, −40 °C. (e) $ArB(OH)_2$, $Pd(PPh_3)_4$, K_3PO_4, toluene/EtOH/H_2O, 100 °C (TBDMS = *tert*-butyldimethylsilyl). (f) TBAF, THF, 0 °C. (g) TMSCN, Et_3N, dioxane, 100 °C. (h) 15% NaOH, 100 °C.

nitrogen atom to give **13** (conditions c), Finkelstein reaction to generate **14** (conditions b) and final bromination (conditions d).[28c] As expected, palladium-catalyzed Suzuki coupling involving bipyridine **12** selectively delivered the functionalized bipyridines **15**–**17** in 2-position with respectively phenyl (**15**), 4-pyridyl (**16**) and *O*-protected 4-phenoxyl (**17**) groups (conditions e).[28c] The remaining bromine in bipyridines **15**–**17** was further exchanged by iodine through Finkelstein reaction to provide compounds **3** and **5** as well as bipyridine **18** (conditions b).[28c] The latter was deprotected to give compound **4** (conditions f).[28b–c] Compound **6** was obtained from **17** through Suzuki coupling to install the 4-pyridyl in 2′-position of **19** and final deprotection (conditions e,f).[28b–c] Compound **7** was prepared in two steps from bipyridine oxide **10**. After reaction of **10** with trimethylsilyl cyanide (TMSCN) (conditions g),[28c] the resulting cyano-bipyridine **20** was hydrolyzed under basic conditions to generate compound **7** (conditions h). The solubility of the carboxylic acid **7** was good enough in methanol to allow its unambiguous characterization by NMR spectroscopy. In particular, the typical chemical shift for the COOH group around 166 ppm was observed by ^{13}C NMR. The characterization data (NMR and HRMS spectra as well as LC traces) for compounds **1**–**7** are provided in the Supporting Information.

Although iodinated heterocyclic compounds were generally described to be relatively unstable due to the high polarizability of the C–I bond, compounds **1**–**5** exhibited high stability, even in solution. In this regard, it is worth noting that the availability of stable iodinated compounds with pharmacological activity is of great interest to provide experimental confirmation of HaB-driven processes occurring at molecular level. On the other hand, experimental data provided by sources other than PDB crystallographic structures are important as benchmark to validate theoretical and computational methods applied to confirm and quantify HaBs identified in biological environment.

Antiproliferative Activity of Iodinated 4,4′-Bipyridines 1, 3 and 4 against Malignant Melanoma Cell Lines

To investigate the antiproliferative activity of the halogenated 4,4′-bipyridine system, we first performed a few explorative dose/response proliferation assays using compounds **1** (R = I, R′ = H), **3** (R = I, R′ = Ph) and **4** (R = I, R′ = *p*-OHC_6H_4) in treating A375, GR-mel (GR), CN-mel (CN), and SK-mel 28 (SK), as malignant melanoma (MM) cell lines, in parallel with the BJ normal fibroblast cell line as control.[39] Cells were treated with 1, 10 or 100 μM concentrations of either **1**, **3** or **4**, up to 24, 48 or 72 h (Figure S1). The results showed a significant dose and time-dependent antiproliferative activity of all three compounds against MM cell lines, while being less effective on BJ control cells.

None of the three compounds showed a significant effect at the 1 μM concentration. At the concentration of 10 μM, compound **1** (Figure S1a) showed to be the most active, being the only one inducing a significant decrease of cell growth on all the MM cell lines after 48 h. Moreover, on A375 cells, it induced 28.1 % growth inhibition ($p < 0.001$), already after 24 h of treatment. The 100 μM concentration was obviously the most toxic dose at any treatment time point and on all the cell lines tested, giving rise for compound **1** to cell growth percentages ranging from 28.1 % (24 h) and 3.0 % (72 h) on A375 cells, to 64.6 % (24 h) and 35.1 % (72 h) on BJ cells. Such a difference of activity between A375 MM cells and BJ control cells was statistically significant ($p < 0.001$). Compound **4** (Figure S1c), at the 10 μM concentration, was able to significantly inhibit cell proliferation after 48 h only on A375 and GR MM cells, even if a significant 22.6 % of inhibition was also observed on GR cells after 24 h. Such activity did not proportionally increase by increasing the time of cells treatment, becoming strong (about 0.0 % of cell growth) only at the concentration of 100 μM, at any experimental time point. Compound **3** (Figure S1b), showed intermediate effects, being significantly active at 10 μM concentration against three MM cell lines (CN, GR, SK) only after 72 h. Additionally, all three compounds showed a significant growth inhibition activity on BJ normal fibroblasts, as control cells, only at the maximum concentration of 100 μM. Compound **1** was the least toxic by allowing 35.1 % of cell growth after the longest experimental treatment time of 72 h. This evidence suggested a good selectivity of compound **1** toward cancer cells. In order to clearly establish which was the most effective compound against melanoma cells, while being the least toxic on normal fibroblasts, we performed exhaustive dose/responses assays which allowed us to calculate the IC_{50} values for the three given compounds on each tested cell line (Table S1) and, consequentially, their selectivity index (SI) [defined as $(IC_{50,BJ})/(IC_{50,MM})$] values (Table S2). Given a compound with antiproliferative capability against a cell line, a SI value ≥ 3 is an indication of its potential suitability as a cancer therapeutic agent.[40] Figure S2 shows the dose/response curves obtained for the most significant cell lines, namely A375 melanoma cells and BJ fibroblast cells as control. Complete results for the remaining three melanoma cell lines, CN, GR, and SK are presented in Figure S3. Compound **1** was confirmed as the most toxic against MM cells, especially for long term treatments, and the least toxic on normal cells (IC_{50} values at 72 h: 5.0 μM and 52.6 μM, respectively on A375 and BJ) with a SI value of 10.5 (Tables S1, S2 and Figure S3a,b). Furthermore, for compound **1** most SI values ≥ 3 were determined among all the experimental points tested (Table S2). Compound **4** also showed a good antiproliferative activity (IC_{50} value at 72 h: 9.1 μM on A375 cell line) (Figure S3e) but SI values ≥ 3 were obtained only at 72 h treatments, while compound **3** was the least active against MM cell proliferation (IC_{50} value at 72 h: 21.3 μM on A375 cell line) (Tables S1 and S2).

Based on the preliminary exploration performed by testing the antiproliferative activities of compounds **1**, **3**, and **4**, A375 proved to be the most sensitive cell line. Thus, the study was deepened by also evaluating compounds **2**, and **5**–**7** with A375 as MM cell line.

Antiproliferative Activity of 4,4′-Bipyridines 2, and 5-7 against A375 Melanoma Cell Line

A375 is a human melanoma cell line, deriving from a very aggressive metastatic tumor,[41] often used as benchmark cell line because of its characteristics and easy availability from American Type Culture Collection (ATCC), so representing a good model for melanoma *in vitro* studies. Indeed, A375 cells carry the oncogene $BRAF^{V600E}$ mutation, the most common mutation associated with MM, and two mutations in the tumor suppressor gene CDKN2 A, a high penetrance melanoma susceptibility gene.[3] It is worth mentioning that some organo-halogen drugs were reported as potent $BRAF^{V600E}$ inhibitors,[24] due to the occurrence of strong HaBs. On this basis, a possible inhibition of $BRAF^{V660E}$ mutation exerted by the iodinated 4,4′-bipyridines could be hypothesized, as well as a HaB-driven enhancement of the antiproliferative activity of **1**, **3** and **4** against A375. Such a hypothesis could also explain the low activity observed on BJ normal fibroblasts, which have a low rate of proliferation and, unlike melanoma cells, do not present a constitutive activation of the proliferative mechanisms driven by $BRAF^{V600E}$ mutation and/or CDKN2 A impairment.

The dose/response curves obtained by treating both A375 MM cells and control BJ fibroblasts with compounds **2**, and **5**–**7** are shown in Figure S4. The IC_{50} and the SI values obtained for all compounds **1**–**7**, after treatments of 24, 48, and 72 h, are summarized in Figure 3. Compound **2** was the most active in inhibiting MM cells proliferation (Figure S4a), surpassing the activity of compound **1** (IC_{50} values at 72 h: 4.2 vs 5.0 μM), and even acting at a shorter incubation time (IC_{50} values at 48 h:

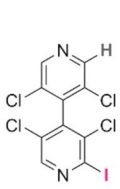

1

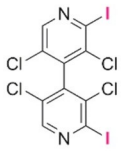

2

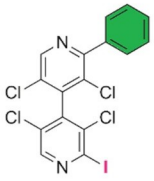

3

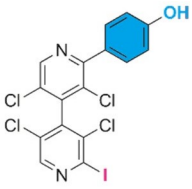

4

Cell lines	time	IC_{50}	CI	SI	IC_{50}	CI	SI	IC_{50}	CI	SI	IC_{50}	CI	SI
A375	24	46.9	[39.5, 56.4]	**4.6**	26.3	[23.4, 29.6]	**3.1**	67.4	[60.5, 75.1]	1.0	30.8	[27.6, 31.4]	2.6
	48	14.7	[13.0, 16.7]	**8.9**	6.0	[5.6, 6.4]	**6.8**	36.9	[34.7, 39.2]	1.8	21.7	[19.5, 24.2]	2.8
	72	5.0	[4.8, 5.3]	**10.5**	4.2	[4.0, 4.5]	**4.2**	21.3	[19.1, 23.7]	2.6	9.1	[8.5, 9.6]	**5.5**
BJ	24	216.4	[138.8, 448.3]		82.4	[67.0, 107.9]		68.0	[63.9, 72.1]		80.9	[76.0, 86.3]	
	48	130.3	[107.7, 170.1]		40.5	[36.6, 44.8]		64.9	[61.0, 68.7]		61.8	[58.2, 65.5]	
	72	52.6	[46.4, 59.3]		17.7	[15.8, 19.9]		56.3	[51.0, 60.9]		49.6	[45.6, 52.6]	

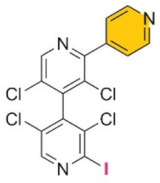

5

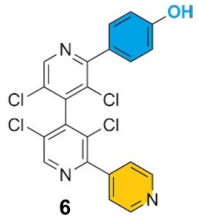

6

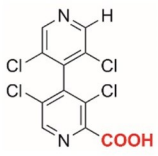

7

Cell lines	time	IC_{50}	CI	SI	IC_{50}	CI	SI	IC_{50}	CI	SI
A375	24	28.8	[26.3, 75.1]	**4.2**	43.7	[40.7, 46.9]	N.D.	>100	--	N.D.
	48	13.5	[12.0, 15.3]	**6.5**	20.2	[18.7, 21.8]	**5.2**	>100	--	N.D.
	72	5.8	[5.5, 6.1]	**9.1**	17.1	[15.5, 18.9]	**5.0**	>100	--	N.D.
BJ	24	122.1	[105.2, 169.8]		nc	--		>100	--	
	48	88.4	[77.7, 108.6]		104.4	[97.4, 118.9]		>100	--	
	72	52.7	[39.8, 70.7]		85.2	[78.2, 93.3]		>100	--	

Figure 3. IC_{50} values [confidence interval, CI], and selectivity Index [$SI = (IC_{50,BJ})/(IC_{50,MM})$] values for compounds **1**–**7** on A375 MM cells and BJ fibroblasts. IC_{50} and 95% CI values are expressed at μM concentration (nc, not calculated) (time, hours). SI values ≥ 3 are highlighted in red. For compound **6** (24 h) and compound **7**, it was not possible to calculate SI values due to their low or absent antiproliferative activity on BJ cells. N.D. = Not determined.

6.0 μM vs 14.7 μM). However, compound **2** showed higher toxicity toward the BJ fibroblasts compared to **1** (IC_{50} values at 72 h: 17.7 vs 52.6 μM, SI 4.2). Compound **5** also showed appreciable antiproliferative activity (IC_{50} value at 72 h: 5.8 μM) (Figure S4c) and good SI (9.1 at 72 h), whereas lower activity was observed for **6** (IC_{50} value at 72 h: 17.1. μM, SI 5.0) (Figure S4e). Compound **7** was ineffective on both A375 and BJ control cells (Figure S4g,h). In all cases, the efficacy of compounds **1**–**6** in inhibiting the growth of the BJ normal cells was significantly lower compared to that exerted on MM cells ($p < 0.001$) (Figures S3b,d,f and S4b,d,f), with SI values often above 3 (Figure 3). These results confirmed a cancer cells selectivity for the antiproliferative activity of these iodinated 4,4′-bipyridines (the statistical significance of the obtained findings on MM cells and BJ control cells proliferation is reported in Tables S3–S6).

Preliminary Data on Apoptosis Induction

One of the principal hallmarks of cancer cells is "resisting cell death": cancer cell loses its capability to trigger apoptosis as a defense mechanism to stop proliferating in case of stress, DNA damage or dysregulation.[42] A common therapeutic anticancer strategy is to rescue such a capability by restoring the defective mechanism of apoptosis induction. The frequent occurrence of clinical chemoresistance in melanoma patients strongly suggests an inactivation of apoptotic pathways in this tumor, and most preclinical single or combination therapy studies share the common aim of reestablishing them.[43] Thus, as compound **1** was shown to be the most active in inhibiting A375 MM cells growth, we also investigated its capability to induce apoptosis by Annexin V and Caspase 3/7 activation tests.

The Annexin-V assay highlights one of the early aspects of the apoptotic process, the phosphatidylserine (PS) exposure on outside the cell membrane. Indeed, Annexin-V binds to PS that externalizes on the surface of apoptotic cells at the beginning of the process.[44] A375 cells were treated with 10, 20 and 40 μM doses of compound **1** for 24, 48 or 72 h, then processed as described in Experimental Section. The results, reported in Figure S5a, showed that compound **1** was able to induce apoptosis in A375 melanoma cells starting from 24 h of treatment at a concentration of 10 μM in about 20% of the cells, raising to 44.4% of apoptotic cells after 72 h of treatment with a 40 μM concentration. Noteworthy, the effects of compound **1** (10 to 40 μM concentration) were not so far from those induced by 0.25 μM Staurosporine (27.1% to 57.9% of apoptotic cells), the pro-apoptotic agent used as a positive control for the experiments. The obtained data evidenced a clear time-dependence for the pro-apoptotic activity of compound **1** that significantly increased after longer incubation times. Otherwise, it did not seem to be dependent on the increasing dose of the compound, probably due to a method bias related to the Annexin-V PS detection assay.

Caspase 3/7 activation is specifically occurring as an advanced apoptosis event. These tests were performed on the A375 cells to confirm the apoptosis induction by compound **1**, already observed with the Annexin-V assays. A375 cells were treated with 20 and 40 μM doses of compound **1** for 24 or 48 h, then processed as described in the Experimental Section. The results, shown in Figure S5b, were comparable to those obtained with the Annexin-V assay, thus confirming the pro-apoptotic activity of compound **1**. In this case, the dose-dependence was more evident, and the effects of compound **1** were visible earlier on caspases' activation: about 40% of apoptotic cells were detected only after 48 h of 40 μM compound **1** treatment.

The results obtained with such two methods were consistent. Annexin V assay is based on detection of PS exposure on cell membranes, with cells that gradually went to die with consequent loss of the signal. Caspases activation assay, instead, is based on detection of cell caspases' enzymatic activity; in apoptotic cells, this proportionally increases, as dose and time of exposure to the apoptotic agent also increase. These differences could explain why the Annexin V assays' results did not evidence a clear dependence of the apoptotic cells detection on the compound **1** doses, which instead was well evidenced by Caspase 3/7 assays. Similarly, Annexin V results showed higher percentages of necrotic cells for any sample (including controls) and the effects of compound **1** on A375 cells appeared to be "slower", in respect to those observed with the Caspase 3/7 assays.

Electrostatic Potential Analysis

Compounds **1**–**7** share the common 3,3′,5,5′-tetrachloro-4,4′-bipyridyl scaffold and the two linked heteroaromatic rings accommodate five (**1** and **7**) or six (**2**-**6**) highly oriented substituents. Among them, compounds **1**–**5** contain electrophilic iodine atoms as substituents of the heteroaromatic core. With the aim to explore and compare the electron charge density distribution on the main interaction sites of compounds **1**–**7**, the V extrema, maxima ($V_{S,max}$) and minima ($V_{S,min}$), were calculated and mapped on 0.002 au electron isodensity surfaces (Table S7). V analysis may give information on specific regions of the molecules with high electron charge density (negative $V_{S,min}$ values), functioning as nucleophiles, or with lower electron charge density (positive $V_{S,max}$ values) working as electrophiles. The iodine electrophilicity is related to the presence of a region of electron charge density depletion, the σ-hole, on its surface, thus, calculated V_S[11b,45] has been widely used as an indicator of the electron anisotropy on iodine.[46] In this frame, the observation of a positive $V_{S,max}$ value on the halogen surface allows for a quantitative estimation of the σ-hole depth which, in turn, is related to the capability of a halogen to behave as a HaB donor (electrophile).

Computation of V_S and related parameters were performed by using Gaussian 09 (DFT, B3LYP, 6-311G*).[47] By comparing the results reported in Table S7, it could be observed that the depth of the σ-hole on the iodine at the 2-position of compounds **1**–**5** was modulated by the distinctive substituent at the 2′-position, with $V_{S,max}$ values ranging from 0.0496 to 0.0536 au. Compounds **1**, **2**, and **5** presented the highest $V_{S,max}$

values on the respective iodine atoms (0.0521, 0.0536, 0.0533 au, respectively) which, consequently, have higher electrophilic character compared to iodine atoms in compounds **3** and **4** (0.0503 and 0.496 au). Differently, compounds **6** and **7** contain HB sites and/or aromatic rings exclusively at the 2,2′-positions of the 4,4′-bipyridyl system. By comparing **1** and **7** (Figure 4), it is worth noting that while the *V* surface calculated for compound **1** (R = I) showed a strong electrophilic region on the iodine σ-hole (blue region) at the 2-position of the heteroaromatic scaffold, a region of high electron charge density centered on the carboxyl oxygen ($V_{S,min} = -0.0578$ au) (red region) could be observed at the same position in compound **7** (R = COOH), along with the electrophilic region of the acidic proton ($V_{S,max} = 0.1104$ au) (blue region). As the COOH group in **7** is free to rotate around the C(2)–C bond, the directionality of the HB sites may change. On the contrary, in compound **1** iodine may exert highly directional HaB through its σ-hole.

Correlation Between Experimental and Computed Results

Compounds **1**–**7** were employed with the aim of evaluating the impact of adding/deleting/substituting the 2-R and 2′-R′ functional groups (Table 1) on the activity against malignant melanoma (MM) cell proliferation, drawing particular attention to the possible contribution of the iodine to this function. Interesting structure-activity correlations emerged by correlating experimental and computational analysis (Figure 5). As shown in Figure 3, the antiproliferative activity against A375 MM cell line, after 72 h treatments, decreased following the order **2** > **1** > **5** > **4** > **6** > **3** > **7**. On this basis, **2** and **1** containing two and one iodine atoms as distinctive substituents resulted as the most active compounds, with the lowest IC_{50} values, while non-iodinated compound **7**, featuring a different structure at the 2-position of the 4,4′-bipyridyl unit, was inactive. On the other hand, by correlating the antiproliferative activity of the iodinated compounds **1**–**5**, in terms of IC_{50} values, and the $V_{S,max}$ on iodine as a measure of its electrophilic capability (Figure 5a), a significant trend was observed. In fact, the antiproliferative activity tended to decrease as the electrophilicity of the iodine atom, featuring each compound, also decreased. Thus, compounds **2**, **1**, and **5** showed higher $V_{S,max}$ values associated to the iodine σ-hole, ranging from 0.0521 to 0.0536 au, compared to **4** and **3**, bearing less electrophilic iodines ($V_{S,max} = 0.0496$ and 0.0503, respectively). Thus, iodine atoms, as substituents, proved to exert a pivotal role on the antiproliferative capability of the corresponding 4,4′-bipyridines. Conversely, the absence of iodine appeared to be detrimental

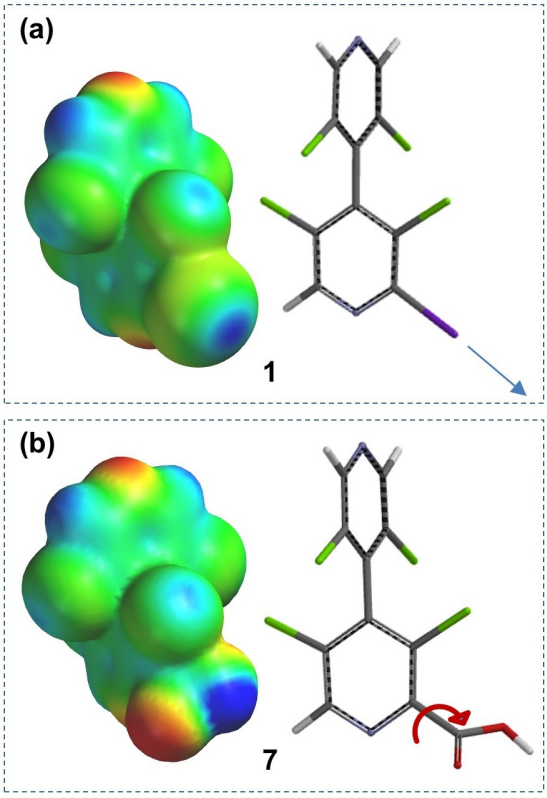

Figure 4. Calculated V_S for compounds **1** (a) and **7** (b). For each compound, tube models are also reported. On the molecule surfaces, electrostatic potential (V_S) > 0 (lower electron charge density) and V_S < 0 (higher electron charge density) are indicated in blue and red, respectively. Intermediate values are in green, yellow, and orange.

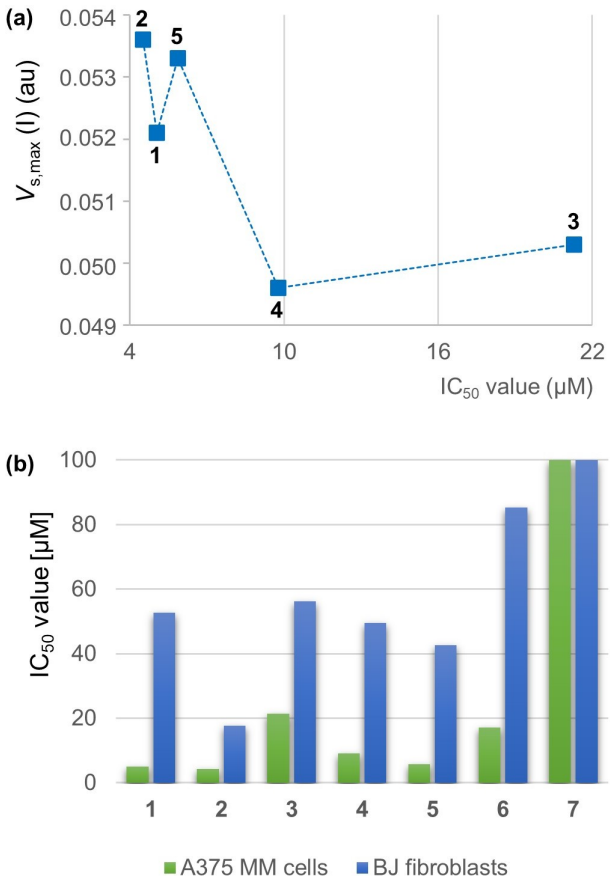

Figure 5. Dependence of IC_{50} average values (μM) on the $V_{S,max}$ of iodine σ-hole calculated for compounds **1**–**5** (a), and toxicity on normal BJ fibroblast (blue) vs A375 MM cells (green) expressed as IC_{50} average values (μM) determined for compounds **1**–**7** (b).

for the antiproliferative activity, the non-iodinated compounds **6** and **7** showing very low activity.

Furthermore, in **3** the presence of a hydrophobic substituent at the 2′-position (R′ = Ph) appeared to be detrimental for the antiproliferative activity compared to compounds **5** and **4** bearing HB sites on the functional group at the 2′-position. Significantly, the superior activity of compound **5** against the MM cells compared to **4** could be also ascribed to the function of the electron-withdrawing 2′-pyridyl group as electronic activator of the electrophilic properties of the 2-iodine.

The HaB is a noncovalent interaction highly directional along the elongation of the C-halogen bond. In a binding pocket, HaB may require more space compared to more flexible (less directional) noncovalent interactions such as hydrogen bond.[48] With the aim of evaluating the size impact of compound **1**–**5** on their antiproliferative activity, we also correlated the antiproliferative activity observed on the A375 MM cell line to the V_S volume calculated for the compounds (Figure S6 and Table S7). Also in this case, a tendency was observed, and the antiproliferative activity appeared to be sensitive to the size of the compounds, compounds **2**, **1**, and **5** being smaller ($274.67 \leq V_S$ volume [Å^3] ≤ 351.77) compared to **4** and **3** (365.77 and 356.87 Å^3, respectively).

Finally, to evaluate the impact of the structural features of the compounds on their specificity toward the MM cells, the toxicity exerted by compounds **1**–**7** on normal BJ fibroblast was compared to that observed for the seven compounds on A375 cells (Figure 5b). Considering compounds **2**, **1**, and **5**, as the most active against MM cells, the diiodinated 4,4′-bipiridine **2** showed higher toxicity on BJ fibroblasts (IC_{50} value 17.7 μM at 72 h, see Figure 3). This behavior may be an obstacle when approaching therapy design, being an indication of low tumor specificity of the potential drug and of possible high systemic toxicity. It is likely that the higher toxicity could be related to the presence of two iodine atoms. This hypothesis could be confirmed by the fact that lower toxicity on fibroblasts was observed for compounds **1** and **3**–**5**.

Conclusions

In the last decade, most information about HaB in biological environment has been accessed by examining crystal structures of protein-ligand complexes extracted from the PDB. In this study, we approach the question by integrating biological and computational analysis. In this frame, substituted 4,4′-bipyridines **1**–**5**, containing iodine atoms activated as electrophiles, were evaluated as inhibitors against CMM cell line proliferation to explore the possible contribution of the iodine atom, as HaB donor, to the biological activity. The structures of compounds **1**–**5** as potential HaB donors functioning in biological environment were selected based on the following remarks: a) the electrophilic features of the iodine atoms were confirmed by electrostatic potential analysis; b) previous studies performed in solution,[29] at the solid state,[28a] and in biological environment[28b] clearly confirmed the HaB-enabled functions of halogenated 4,4′-bipyridines.

As a result of this study, 4,4′-bipyridine **1** showed almost the same toxicity on A375 than **2** (IC_{50} values: 5.0 μM vs 4.2 μM at 72 h), but much lower toxicity on control BJ fibroblasts (IC_{50} value 52.6 μM at 72 h) (SI 10.5), proving to be a better candidate to develop new therapeutic strategies. Otherwise, for compound **2**, the presence of a second iodine atom on the 4,4′-bipyridine unit appeared detrimental for the BJ fibroblast viability (IC_{50} value 17.7 μM). Significantly, non-iodinated compounds **6** and **7**, used as reference for comparison showed poor antiproliferative activity.

Furthermore, although these results are not exhaustive, a preliminary evaluation of iodinated 4,4′-bipyridine **1**, as pro-apoptotic agent, was also performed by using two different techniques. The obtained results suggested that MM cell death induced by **1** might be, at least partially, attributable to apoptosis, with a pro-apoptotic activity comparable to that exerted by Staurosporin, as positive control. On these bases, we are planning to extend the analysis to other iodinated 4,4′-bipyridines by also studying in deep other aspects of the apoptosis event, like mitochondrial membrane polarization, and by comparison with the effect on control normal cells.

The results obtained herein confirmed the high potential of iodinated compounds in designing novel anti-melanoma therapeutics strategies, paving the way for a new perspective in this field.

Experimental Section

The following compounds were prepared according to literature procedures: **9a**;[28a] **1** and **3**–**5**;[28b] **9b**, **10**–**15**, **17**–**20** and **6**.[28c]

Synthesis of Compound 2

In a dry tube were placed bipyridine **11** (0.268 mmol, 100 mg), NaI (0.536 mmol, 80.4 mg), CuI (0.0268 mmol, 5.1 mg) and *trans-N,N′*-dimethylcyclohexane-1,2-diamine (0.0536 mmol, 7.6 mg). The tube was evacuated and filled with argon before addition of degassed dioxane (2 mL). The tube was sealed with a screw cap and heated at 120 °C for 60 h. After cooling to room temperature, NH_4OH (4 mL) and H_2O (8 mL) were added then the product was extracted with dichloromethane (3×10 mL). After drying over $MgSO_4$, filtration and concentration, the crude compound was purified by chromatography on silica gel (pentane/CH_2Cl_2 7/3) to give compound **2** as a white solid (75 mg, 67 %). ^{1}H NMR (500 MHz, $CDCl_3$) δ 8.67 (s, 2H), 8.46 (s, 1H). ^{13}C NMR (126 MHz, $CDCl_3$) δ 148.0; 147.8; 140.6; 140.3; 137.3; 131.2; 130.9; 119.5. HRMS (ESI-TOF) $[M+H]^+$ *m/z*: Calcd. for $C_{10}H_3Cl_4IN_2$ 418.8168, found: 418.8152.

Synthesis of Compound 16

In a dry tube were placed bipyridine **12** (0.5 mmol, 257 mg), $Pd(PPh_3)_4$ (0.025 mmol, 29 mg), 4-pyridinylboronic acid (90 % purity, 0.55 mmol, 68 mg) and K_3PO_4 (0.25 mmol, 53 mg). The tube was evacuated and filled with argon before addition of degassed mixture of toluene/water/ethanol (6:1:1, 6 mL). The tube was sealed with a screw cap and heated at 100 °C for 15 h. The cooled reaction mixture was diluted with water (15 mL) and extracted with CH_2Cl_2 (3×20 mL). After drying over $MgSO_4$, filtration and concentration, the crude compound was purified by chromatography on silica gel (pentane/ethyl acetate 7/3) to give compound **16** as a

colorless syrup (157 mg, 69%). ^{1}H NMR (500 MHz, $CDCl_3$) δ 8.79 (m, 3H), 8.50 (s, 1H), 7.71 (d, J = 5.0 Hz, 2H). ^{13}C NMR (126 MHz, $CDCl_3$) δ 153.3, 150.1, 148.0, 147.9, 144.6, 142.4, 140.8, 137.2, 131.1, 130.7, 129.1, 124.0, 119.5. HRMS (ESI-TOF) $[M+H]^+$ *m/z*: Calcd. for $C_{15}H_7Cl_4IN_3$ 495.8433, found: 494.8400.

Synthesis of Compound 7

A resealable tube was charged with bipyridine **20**[28c] (0.219 mmol, 70 mg) and a solution of NaOH (15% in H_2O, 2 mL) was added. The tube was sealed and heated at 100 °C for 16 h. After cooling to room temperature, HCl 2 M was added until pH <4 and the mixture was extracted with diethyl ether (4×5 mL). The combined organic phases were dried over Na_2SO_4. After filtration and concentration under vacuum, bipyridine **7** was obtained as a white powder (67 mg, 90%). ^{1}H NMR (CD_3OD, 500 MHz) δ 8.83 (s, 1H), 8.80 (s, 2H) ppm; ^{13}C NMR (CD_3OD, 126 MHz) δ 166.4, 149.6, 149.2, 148.5, 143.2, 141.3, 134.0, 132.3, 130.4 ppm. HRMS (ESI-TOF): m/z calcd for $C_{11}H_3Cl_4N_2O_2$ $[M-H]^-$: 334.8954; found: 334.8971.

Cell Based Assays

Four malignant melanoma (MM) cell lines have been used as a multiple experimental *in vitro* model for this study. They have been chosen among 27 lines collected in our laboratory, as the most suitable to represent different molecular types of melanoma:[39] 1) A375 (CVCL_0132), derived from melanoma cutaneous metastasis,[41] carrying the $CDKN2A^{E61*-E69*}$ and $BRAF^{V600E}$ gene mutations,[49] 2) CN-mel (CN) (CVCL_7037), derived from melanoma lymph node metastasis, carrying the $NRAS^{Q61R}$ gene mutation, 3) GR-mel (GR) (CVCL_G320), derived from a primary melanoma, carrying a homozygous deletion in the CDKN2B gene, 4) SK-mel 28 (SK) (CVCL_0526), derived from melanoma lymph node metastasis, carrying the $PTENT^{167A}$ gene mutation. As a non-tumor control, we used a human fibroblast cell line from a healthy donor, the BJ cell line, purchased by American Type Culture Collection (ATCC®, CRL-2522™). CN, GR and SK MM cell lines were kindly donated by the Istituto Dermopatico dell'Immacolata (IDI, Rome, Italy). A375 MM cell line was also purchased by ATCC® (CRL-1619TM). All cell lines were cultured in RPMI medium with stable glutamine, supplemented with 10% fetal bovine serum (FBS) and penicillin/streptomycin (1 U/mL) (complete medium), in a humidified atmosphere with 5% CO_2, at 37 °C.

Bipyridine compounds **1**–**7** were dissolved as 100 mM stock solutions with dimethyl sulfoxide (DMSO) and stored as 50 μL aliquots at −20 °C until use. Compound working dilutions were prepared using complete medium, immediately before use, so that they contained <0.1% DMSO final concentration.

Cells were seeded in 96-well plates, RPMI culture medium with stable glutamine, supplemented with 10% fetal bovine serum (FBS) and penicillin/streptomycin (1 U/mL) (complete medium), and grown in a humidified atmosphere with 5% CO_2, at 37 °C. After 24 h, the medium was replaced by complete medium supplemented or not (control) with increasing concentrations of any of **1**–**7** compounds. Cells were grown up to 24, 48 or 72 h and the medium was replaced every 48 h (for 72 h assays). Cell viability was finally determined by MTT assay[50] as described previously.[51] All experiments were performed in quadruplicate and repeated at least three times. Details about the IC_{50} values calculation and the statistical analysis for the MMT proliferation assays are provided as Supporting information.

The selectivity index (SI) was calculated by dividing the IC_{50} value determined for the activity of compounds **1**–**7** on BJ fibroblasts by the IC_{50} value determined for MM cells for each experimental point. SI was considered as interesting for values higher than 3.

Experimental details about the apoptosis assays in the A375 MM cells by Annexin V and Caspase 3/7 activation tests are provided as Supporting Information.

Calculation of Electrostatic Potential

For compound **7**, conformational search was performed employing the density functional theory (DFT) method with the B3LYP functional and the 6–311G* basis set, and the Spartan' 10 Version 1.1.0 (Wavefunction Inc., Irvine, CA, USA) program.[52] Geometry optimization and computation of V mapped on a 0.002 au isodensity surface (V_S) and related parameters (V_S extrema, $V_{S,max}$ and $V_{S,min}$ values, given in au) were performed by using Gaussian 09 (DFT, B3LYP, 6–311G*) (Wallingford, CT, USA).[47] In this regard, it is worth mentioning that, given a molecule, the $V(\mathbf{r})$ at each point **r** in the surrounding space, is created by each nucleus (first positive term) and electron (second negative term) of the molecule and given by equation (1)

$$V(\mathbf{r}) = \sum_A \frac{Z_A}{R_A - \mathbf{r}} - \int \frac{\rho(\mathbf{r})d\mathbf{r}'}{|\mathbf{r}' - \mathbf{r}|} \quad (1)$$

where Z_A is the charge on nucleus A located at R_A, and $\rho(\mathbf{r})$ is the electron density function.[45] Thus, the sign of V may be positive or negative depending on the dominant contribution, which is positive and negative from nuclei and electrons, respectively. Search for the exact location of such $V_{S,max}$ and $V_{S,min}$ was made through the Multiwfn code[53a] and through its module enabling quantitative analyses of molecular surfaces (isovalue 0.002).[53b] For the V_S representations, colors towards red depict negative V_S, while colors towards blue depict positive V_S, and colors in be-tween (orange, yellow, green) depict intermediate values. As part of our previous research,[28b,29c] this methodology was also used for compounds **1**–**6** to obtain the V values reported in Table S7.

Supporting Information

Synthesis of **1**–**7**: ^{1}H and ^{13}C NMR spectra, HRMS spectra, and LC traces.

Figure S1. Explorative dose/response assays for compounds **1**, **3** and **4**.

Table S1. IC_{50} values for compounds **1**, **3**, **4** on four MM cell lines and BJ fibroblast cell line.

Table S2. Selectivity Index values for compounds **1**, **3** and **4** for A375, CN, GR, and SK cell lines.

Figure S2. Antiproliferative activity of compounds **1**, **3** and **4** on A375 and BJ cell lines.

Figure S3. Antiproliferative activity of **1**, **3** and **4** on CN, GR and SK MM cell lines.

Figure S4. Antiproliferative activity of compounds **2** and **5**–**7** on A375 and BJ cell lines.

Table S3. Dose dependence of **1**–**7** activity: Student's T test.

Table S4. Selectivity of compounds **1**–**7** to MM cells: Holm-Sidak test.

Table S5. Time dependence of **1**–**7** activity: Holm-Sidak test.

Table S6. Selectivity of compounds **1**, **3** and **4** to CN, GR and SK MM cells: Holm-Sidak test.

Figure S5. Pro-apoptotic activity of compound **1**.

Table S7. $V_{S,max}$ and $V_{S,min}$ (au) (isovalue = 0.002 au) and V_S volume (Å^3) calculated for **1**–**7**.

Figure S6. Dependence of IC_{50} (μM) on the surface volume calculated for compounds **1**–**5**.

Experimental Section: Additional details.

Acknowledgements

The authors sincerely thank Dr. Stefania D'Atri and Dr. Lauretta Levati from "Istituto Dermopatico dell'Immacolata-IRCCS" (IDI), Rome, ITALY, for providing the primary MM cell lines CN-mel, GR-mel and SK-mel 28. This research was partially funded by Grant "AIRC 5 per mille 2018 – Id. 21073 program". The authors also thank CNR (Grant no.: SAC.AD002.011.032), the University of Strasbourg, the Centre National de la Recherche Scientifique (CNRS), and the French National Research Agency (Grant no.: ANR-21-CE07-0014) for financial support.

Conflict of Interests

The authors declare no conflict of interest.

Data Availability Statement

The data that support the findings of this study are available from the corresponding author upon reasonable request.

Keywords: Antiproliferation · Bipyridine · Halogen bond · Melanoma · Molecular modeling

[1] F. Zamagni, L. Bucchi, S. Mancini, E. Crocetti, L. Dal Maso, S. Ferretti, A. Biggeri, S. Villani, F. Baldacchini, O. Giuliani, A. Ravaioli, R. Vattiato, A. Brustolin, G. Candela, S. Carone, G. Carrozzi, R. Cavallo, Y. M. Dinaro, M. Ferrante, S. Iacovacci, G. Mazzoleni, A. Musolino, R. V. Rizzello, D. Serraino, F. Stracci, R. Tumino, C. Masini, L. Ridolfi, G. Palmieri, I. Stanganelli, F. Falcini, *Br. J. Dermatol.* **2022**, *187*, 52–63.
[2] G. V. Long, S. M. Swetter, A. M. Menzies, J. E. Gershenwald, R. A. Scolyer, *Lancet* **2023**, *402*, 485–502.
[3] G. Palmieri, M. Colombino, M. Casula, A. Manca, M. Mandalà, A. Cossu, *Curr. Oncol. Rep.* **2018**, *20*, 86.
[4] L. M. Parra, R. M. Webster, *Nat. Rev.* **2022**, *21*, 489–490.
[5] P. Kozyra, D. Krasowska, M. Pitucha, *Int. J. Mol. Sci.* **2022**, *23*, 6084.
[6] M. Matias, J. O. Pinho, M. J. Penetra, G. Campos, C. P. Reis, M. M. Gaspar, *Cells* **2021**, *10*, 3088.
[7] a) M. Pennisi, G. Russo, V. Di Salvatore, S. Candido, M. Libra, F. Pappalardo, *Expert Opin. Drug Discovery* **2016**, *11*, 609–621; b) D. Prada-Gracia, S. Huerta-Yépez, L. M. Moreno-Vargas, *Bol. Med. Hosp. Infant. Mex.* **2016**, *73*, 411–423; c) S. Cui, A. Aouidate, S. Wang, S. Yu, Y. Li, S. Yuan, *Front. Pharmacol.* **2020**, *11*, 733.
[8] a) P. Peluso, B. Chankvetadze, *Chem. Rev.* **2022**, *122*, 13235–13400; b) C. Bissantz, B. Kuhn, M. Stahl, *J. Med. Chem.* **2010**, *53*, 5061–5084.
[9] D. Herschlag, M. M. Pinney, *Biochemistry* **2018**, *57*, 3338–3352.
[10] K. A. Wilson, R. W. Kung, S. D'souza, S. D. Wetmore, *Nucleic Acids Res.* **2021**, *49*, 2213–2225.
[11] a) A. L. Kantsadi, J. M. Hayes, S. Manta, V. T. Skamnaki, C. Kiritsis, A.-M. G. Psarra, Z. Koutsogiannis, A. Dimopoulou, S. Theofanous, N. Nikoleousakos, P. Zoumpoulakis, M. Kontou, G. Papadopoulos, S. E. Zographos, D. Komiotis, D. D. Leonidas, *ChemMedChem* **2012**, *7*, 722–732; b) R. Wilcken, M. O. Zimmermann, A. Lange, A. C. Joerger, F. M. Boeckler, *J. Med. Chem.* **2013**, *56*, 1363–1388.
[12] O. Carugo, G. Resnati, P. Metrangolo, *ACS Chem. Biol.* **2021**, *16*, 1622–1627.
[13] H. S. Biswal, A. K. Sahu, A. Frontera, A. Bauzá, *J. Chem. Inf. Model.* **2021**, *61*, 3945–3954.
[14] A. Bauzá, A. Frontera, T. J. Mooibroek, *Chem. Eur. J.* **2019**, *25*, 13436–13443.
[15] K. E. Riley, P. Hobza, *WIREs Comput. Mol. Sci.* **2011**, *1*, 3–17.
[16] A. Lange, M. Günther, F. M. Büttner, M. O. Zimmermann, J. Heidrich, S. Hennig, S. Zahn, C. Schall, A. Sievers-Engler, F. Ansideri, P. Koch, M. Laemmerhofer, T. Stehle, S. A. Laufer, F. M. Boeckler, *J. Am. Chem. Soc.* **2015**, *137*, 14640–14652.
[17] Z.-L. Deng, C.-X. Du, X. Li, B. Hu, Z.-K. Kuang, R. Wang, S.-Y. Feng, H.-Y. Zhang, D.-X. Kong, *J. Chem. Inf. Model.* **2013**, *53*, 2820–2828.
[18] a) Z. Xu, Z. Yang, Y. Liu, Y. Lu, K. Chen, W. Zhu, *J. Chem. Inf. Model.* **2014**, *54*, 69–78; b) P. S. Ho, *Future Med. Chem.* **2017**, *9*, 637–640; c) L. Mendez, G. Henriquez, S. Sirimulla, M. Narayan, *Molecules* **2017**, *22*, 1397; d) J. Heidrich, L. E. Sperl, F. M. Boeckler, *Front. Chem.* **2019**, *7*, 9.
[19] G. Cavallo, P. Metrangolo, R. Milani, T. Pilati, A. Priimagi, G. Resnati, G. Terraneo, *Chem. Rev.* **2016**, *116*, 2478–2601.
[20] K. Mu, Z. Zhu, A. Abula, C. Peng, W. Zhu, Z. Xu, *J. Med. Chem.* **2022**, *65*, 4424–4435.
[21] S. Sirimulla, J. B. Bailey, R. Vegesna, M. Narayan, *J. Chem. Inf. Model.* **2013**, *53*, 2781–2791.
[22] A. Chopra, J. D. Bauman, F. X. Ruiz, E. Arnold, *J. Med. Chem.* **2023**, *66*, 6013–6024.
[23] D. J. Wood, J. D. Lopez-Fernandez, L. E. Knight, I. Al-Khawaldeh, C. Gai, S. Lin, M. P. Martin, D. C. Miller, C. Cano, J. A. Endicott, I. R. Hardcastle, M. E. M. Noble, M. J. Waring, *J. Med. Chem.* **2019**, *62*, 3741–3752.
[24] Y. Li, B. Guo, Z. Xu, B. Li, T. Cai, X. Zhang, Y. Yu, H. Wang, J. Shi, W. Zhu, *Sci. Rep.* **2016**, *6*, 31074.
[25] P. Kozyra, A. Korga-Plewko, Z. Karczmarzyk, A. Hawrył, W. Wysocki, M. Człapski, M. Iwan, M. Ostrowska-Lésko, E. Fornal, M. Pitucha, *Biomol. Eng.* **2022**, *12*, 151.
[26] T. Q. Pham, I. Greguric, X. Liu, P. Berghofer, P. Ballantyne, J. Chapman, F. Mattner, B. Dikic, T. Jackson, C. Loc'h, A. Katsifis, *J. Med. Chem.* **2007**, *50*, 3561–3572.
[27] J. Rouanet, M. Quintana, P. Auzeloux, F. Cachin, F. Degoul, *Pharmacol. Ther.* **2021**, *224*, 107829.
[28] a) V. Mamane, P. Peluso, E. Aubert, S. Cossu, P. Pale, *J. Org. Chem.* **2016**, *81*, 4576–4587; b) A. Dessì, P. Peluso, R. Dallocchio, R. Weiss, G. Andreotti, M. Allocca, E. Aubert, P. Pale, V. Mamane, S. Cossu, *Molecules* **2020**, *25*, 2213; c) E. Aubert, E. Wenger, P. Peluso, V. Mamane, *Compounds* **2021**, *1*, 58–74.
[29] a) P. Peluso, V. Mamane, A. Dessì, R. Dallocchio, E. Aubert, C, Gatti, D. Mangelings, S. Cossu, *J. Chromatogr. A* **2020**, *1616*, 460788; b) R. Dallocchio, B. Sechi, A. Dessì, B. Chankvetadze, S. Cossu, V. Mamane, R. Weiss, P. Pale, P. Peluso, *Electrophoresis* **2021**, *42*, 1853–1863; c) R. Dallocchio, A. Dessì, B. Sechi, B. Chankvetadze, S. Cossu, V. Mamane, E. Aubert, C. Rozzo, G. Palmieri, Y. Spissu, P. Peluso, *J. Chromatogr. Open* **2022**, *2*, 100030.
[30] V. Cody, P. Murray-Rust, *J. Mol. Struct.* **1984**, *112*, 189–199.
[31] L. D. Pennington, D. T. Moustakas, *J. Med. Chem.* **2017**, *60*, 3552–3579.
[32] F. U. Rahman, A. Ali, I. U. Khan, M. Z. Bhatti, M. Petroselli, H.-Q. Duong, J. Martì-Rujas, Z.-T. Li, H. Wang, D.-W. Zhang, *Inorg. Chem. Commun.* **2019**, *102*, 95–103.
[33] S. Wang, H. Wu, F. Chen, Y. Zhang, Y. Zhang, B. Sun, *RSC Adv.* **2019**, *9*, 33023–33028.
[34] a) D. E. Smith, I. Marquez, M. E. Lokensgard, A. L. Rheingold, D. A. Hecht, J. L. Gustafson, *Angew. Chem. Int. Ed.* **2015**, *54*, 11754–11759; b) M. Basilaia, M. H. Chen, J. Secka, J. L. Gustafson, *Acc. Chem. Res.* **2022**, *55*, 2904–2919.
[35] K. Dodou, R. J. Anderson, W. J. Lough, D. A. P. Small, M. D. Shelley, P. W. Groundwater, *Bioorg. Med. Chem.* **2005**, *13*, 4228–4237.
[36] S. A. Foster, D. M. Whalen, A. Özen, M. J. Wongchenko, J. P. Yin, I. Yen, G. Schaefer, J. D. Mayfield, J. Chmielecki, P. J. Stephens, L. A. Albacker, Y. Yan, K. Song, G. Hatzivassiliou, C. Eigenbrot, C. Yu, A. S. Shaw, G. Manning, N. J. Skelton, S. G. Hymowitz, S. Malek, *Cancer Cell* **2016**, *29*, 477–493.
[37] a) M. Pisano, G. Pagnan, M. A. Dettori, S. Cossu, I. Caffa, I. Sassu, L. Emionite, D. Fabbri, M. Cilli, F. Pastorino, G. Palmieri, G. Delogu, M. Ponzoni, C. Rozzo, *Mol. Cancer* **2010**, *9*, 137; b) M. A. Dettori, M. Pisano, C. Rozzo, G. Delogu, D. Fabbri, *ChemMedChem* **2021**, *16*, 1022–1033;

c) M. Pisano, M. A. Dettori, D. Fabbri, G. Delogu, G. Palmieri, C. Rozzo, *Int. J. Mol. Sci.* **2021**, *22*, 5636.
[38] S. L. Kidd, E. Fowler, T. Reinhardt, T. Compton, N. Mateu, H. Newman, D. Bellini, R. Talon, J. McLoughlin, T. Krojer, A. Aimon, A. Bradley, M. Fairhead, P. Brear, L. Díaz-Sáez, K. McAuley, H. F. Sore, A. Madin, D. H. O'Donovan, K. V. M. Huber, M. Hyvönen, F. von Delft, C. G. Dowson, D. R. Spring, *Chem. Sci.* **2020**, *11*, 10792–10801.
[39] M. Casula, A. Muggiano, A. Cossu, M. Budroni, C. Caracò, P. A. Ascierto, E. Pagani, I. Stanganelli, S. Canzanella, M. C. Sini, G. Palomba, G. Palmieri, *BMC Cancer* **2009**, *9*, 352.
[40] a) W. Supasena, C. Muangnoi, K. Praengamc, T. W. Wongd, G. Qiue, S. Ye, J. Wu, S. Tanasupawat, P. Rojsitthisak, *Eur. Polym. J.* **2020**, *141*, 110056; b) C. Bézivin, S. Tomasi, F. Lohézic-Le Dévéhat, J. Boustie, *Phytomedicine* **2003**, *10*, 499–503.
[41] D. J. Giard, S. A. Aaronson, G. J. Todaro, P. Arnstein, J. H. Kersey, H. Dosik, W. P. Parks, *J. Natl. Cancer Inst.* **1973**, *51*, 1417–1423.
[42] D. Hanhan, *Cancer Discov.* **2022**, *12*, 31–46.
[43] J. Eberle, L. F. Fecker, A. M. Hossini, B. M. Kurbanov, H. Fechner, *Exp. Dermatol.* **2008**, *17*, 1–11.
[44] M. van Engeland, L. J. Nieland, F. C. Ramaekers, B. Schutte, C. P. Reutelingsperger, *Cytometry* **1998**, *31*, 1–9.
[45] E. Scrocco, J. Tomasi, *Top. Curr. Chem.* **1973**, *42*, 95–170.
[46] J. Heidrich, T. E. Exner, F. M. Boeckler, *J. Chem. Inf. Model.* **2019**, *59*, 636–643.
[47] M. J. Frisch, G. W. Trucks, H. B. Schlegel, G. E. Scuseria, M. A. Robb, J. R. Cheeseman, G. Scalmani, V. Barone, B. Mennucci, G. A. Petersson, H. Nakatsuji, M. Caricato, X. Hratchian, H. P. Li, A. F. Izmaylov, J. Bloino, G. Zheng, J. L. Sonnenberg, M. Hada, M. Ehara, K. Toyota, R. Fukuda, J. Hasegawa, M. Ishida, T. Nakajima, Y. Honda, O. Kitao, H. Nakai, T. Vreven, J. A. Montgomery Jr, J. E. Peralta, F. Ogliaro, M. Bearpark, J. J. Heyd, E. Brothers, K. N. Kudin, V. N. Staroverov, T. Keith, R. Kobayashi, J. Normand, K. Raghavachari, A. Rendell, J. C. Burant, S. S. Iyengar, J. Tomasi, M. Cossi, N. Rega, J. M. Millam, M. Klene, J. E. Knox, J. B. Cross, V. Bakken, C. Adamo, J. Jaramillo, R. Gomperts, R. E. Stratmann, O. Yazyev, A. J. Austin, R. Cammi, C. Pomelli, J. W. Ochterski, R. L. Martin, K. Morokuma, V. G. Zakrzewski, G. Voth, P. Salvador, J. J. Dannenberg, S. Dapprich, A. D. Daniels, O. Farkas, J. B. Foresman, J. Ortiz, J. Cioslowski, D. J. Fox, Gaussian 09, Revision B. 01; Gaussian, Inc.: Wallingford, CT, USA, 2010.
[48] P. Politzer, J. S. Murray, T. Clark, *Phys. Chem. Chem. Phys.* **2010**, *12*, 7748–7757.
[49] F. G. Cordaro, A. L. De Presbiteris, R. Camerlingo, N. Mozzillo, G. Pirozzi, E. Cavalcanti, A. Manca, G. Palmieri, A. Cossu, G. Ciliberto, *Oncol. Rep.* **2017**, *38*, 2741–2751.
[50] a) T. Mosmann, *J. Immunol. Methods* **1983**, *65*, 55–63; b) P. Kumar, A. Nagarajan, P. D. Uchil, *Cold Spring Harb. Protoc.* **2018**, *2018*, 6.
[51] C. Rozzo, D. Sanna, E. Garribba, M. Serra, A. Cantara, G. Palmieri, M. Pisano, *J. Inorg. Biochem.* **2017**, *174*, 14–24.
[52] Y. Shao, L. F. Molnar, Y. Jung, J. Kussmann, C. Ochsenfeld, S. T. Brown, A. T. B. Gilbert, L. V. Slipchenko, S. V. Levchenko, D. P. O'Neil, R. A. Di Stasio Jr, R. C. Lochan, T. Wang, G. J. O. Beran, N. A. Besley, J. M. Herbert, C. Y. Lin, T. VanVoorhis, S. H. Chien, A. Sodt, R. P. Steele, V. A. Rassolov, P. E. Maslen, P. P. Korambath, R. D. Adamson, B. Austin, J. Baker, E. F. C. Byrd, H. Dachsel, R. J. Doerksen, A. Dreuw, B. D. Dunietz, A. D. Dutoi, T. R. Furlani, S. R. Gwaltney, A. Heyden, S. Hirata, C.-P. Hsu, G. Kedziora, R. Z. Khalliulin, P. Klunzinger, A. M. Lee, M. S. Lee, W. Z. Liang, I. Lotan, N. Nair, B. Peters, E. I. Proynov, P. A. Pieniazek, Y. M. Rhee, J. Ritchie, E. Rosta, C. D. Sherrill, A. C. Simmonett, J. E. Subotnik, H. L. Woodcock III, W. Zhang, A. T. Bell, A. K. Chakraborty, D. M. Chipman, F. J. Keil, A. Warshel, W. J. Hehre, H. F. Schaefer, J. Kong, A. I. Krylov, P. M. W. Gill, M. Head-Gordon, *Phys. Chem. Chem. Phys.* **2006**, *8*, 3172–3191.
[53] a) T. Lu, F. Chen, *J. Comp.Chem.* **2012**, *33*, 580–592; b) T. Lu, F. Chen, *J. Mol. Graphics Modell.* **2012**, *38*, 314–323.

Manuscript received: November 27, 2023
Revised manuscript received: March 14, 2024
Accepted manuscript online: March 15, 2024
Version of record online: ■■, ■■

RESEARCH ARTICLE

The antiproliferative activity of seven substituted 3,3′,5,5′-tetrachloro-4,4′-bipyridines was evaluated against malignant melanoma (MM) cell lines. The 3,3′,5,5′-tetrachloro-2-iodo-4,4′-bipyridine showed high activity on A375, and very low toxicity on control BJ fibroblasts. *In silico* studies confirmed the highest electrophilic properties for the iodine atoms contained in the most active compounds against MM cell line proliferation.

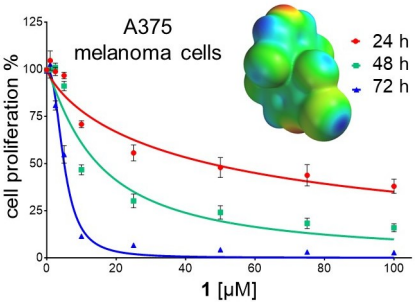

Dr. P. Peluso, Dr. V. Mamane*, Dr. Y. Spissu, G. Casu, A. Dessì, R. Dallocchio, B. Sechi, Prof. G. Palmieri, Dr. C. Rozzo**

1 – 13

Iodinated 4,4′-Bipyridines with Antiproliferative Activity Against Melanoma Cell Lines